Axial Position Control of a Lorentz-Force-Type Cylindrical Self-Bering Motor with Coreless Distributed Windings

Satoshi UENO[a], Koki MAEDA[a], Chengyan ZHAO[a]

a Ritsumeikan University, 1-1-1 Nojihigashi, Kusatsu, Shiga, Japan, sueno@se.ritsumei.ac.jp

Abstract

A Lorentz-force-type self-bearing motor rotates and supports a rotor using the Lorentz force generated by the magnetic flux from the rotor's permanent magnets and the current flowing in the stator windings. In the previous model, only rotational torque and radial forces were controlled by two coreless cylindrical six-phase distributed windings. This paper proposes a method to control the axial force using two diamond-shaped windings. The structure and control principle is introduced, then a prototype machine and the result of the levitation test are shown.

Keywords: Self-bearing motor, Lorentz force, Axial force, Levitation control

1. Introduction

A self-bearing motor (SBM) integrates a motor and magnetic bearings and is possible to reduce the overall size and cost of the device. As an application example, a blood pump using the SBM has been developed (Osa et al. 2021). Although various types of SBMs have been proposed, this study focuses on a Lorentz-force-type cylindrical SBM (L-SBM) with coreless six-phase distributed windings (Ueno et al. 2009). Conventional L-SMBs cannot control the axial force, then it is necessary to use the passive stability provided by a thin rotor (Steinert et al. 2014) or add an active magnetic bearing (Ren & Stephens 2005) to support the axial direction of the rotor. When passive stability is used, the shape of the rotor is limited, and when active magnetic bearings are used, the structure becomes complicated.

In this study, we propose a winding structure that enables control of the axial direction in addition to the motor torque and radial direction. By generating and controlling the axial force, an axial magnetic bearing can be removed, thus it is possible to further miniaturization and simplification. This paper describes the structure of the proposed motor, the principle and analysis of the bearing force

This paper describes the structure of the proposed motor, the principle of generating the bearing force, and the results of the bearing force analysis. The results of the levitation test on the prototype machine are also shown.

2. Structure and principle

2.1 Structure

Fig. 1 shows the structure of the proposed LSBM. Two coreless distributed windings are vertically arranged in the stator. The rotor consists of an iron core and permanent magnets, whose axial length overlaps the lower half of the upper coil and the upper half of the lower coil. In this paper, four PMs are attached, and the number of poles of the rotor is four.

Fig. 2 shows the development view of the stator winding. It consists of six-phase diamond-shaped windings and is rounded into a cylindrical shape to attach to the stator. Since the winding in this overlapping area is

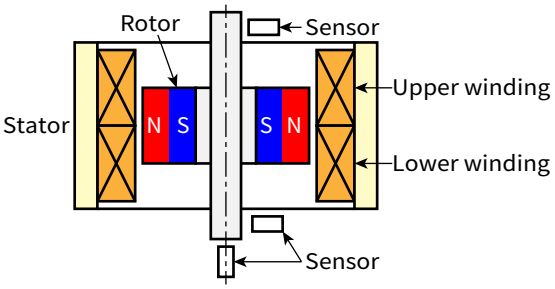

Figure 1: Structure of the proposed motor.

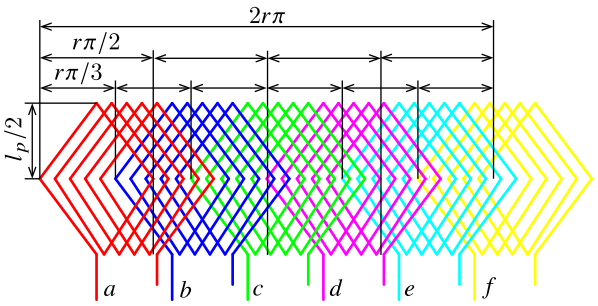

Figure 2: Development view of a six-phase winding.

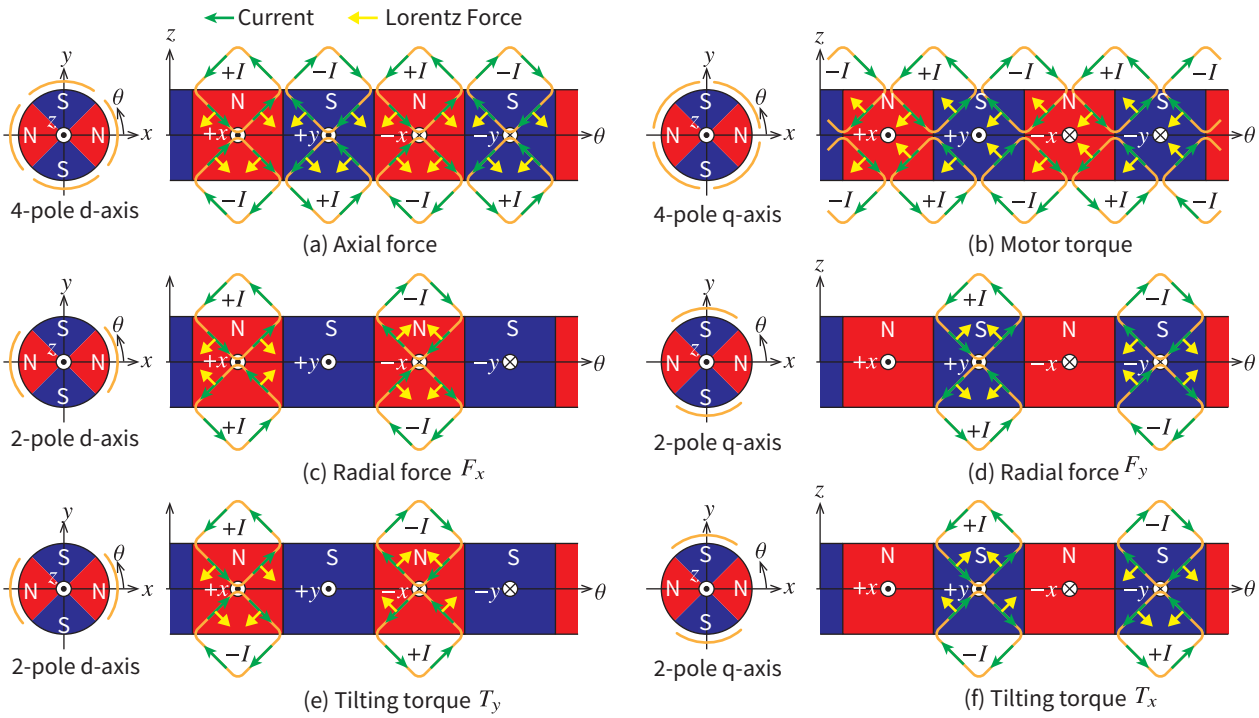

Figure 3: Generation of force and torque.

oblique, it can generate axial force. The width of a phase is $r\,\pi/2$, and the space between phases is $r\,\pi/3$, where r is the radius of the winding and l_p is the axial length of the PMs.

2.2 Generation of force and torque

The principle of control force generation is shown in Fig. 3. The right figure shows the top view, and the left figure shows the developed view. The red and blue represent the N- and S-pole, and the N-pole generating magnetic flux from the back of the paper to the front. For simplicity, only one winding in the d- and q-axis direction is shown. The green lines indicates the direction of the currents, and the yellow line indicates the direction of the Lorentz forces.

As shown in Fig. 3 (a), the axial force is generated by suppling the four-pole d-axis currents in opposite direction between the upper and lower windings. Since the tangential forces are cancelled, only the axial force is generated. The motor torque is generated by four-pole q-axis current as shown in Fig. 3 (b). Radial forces and tilting torques are generated by two-pole current as shown in Figs. 3 (c) - (f).

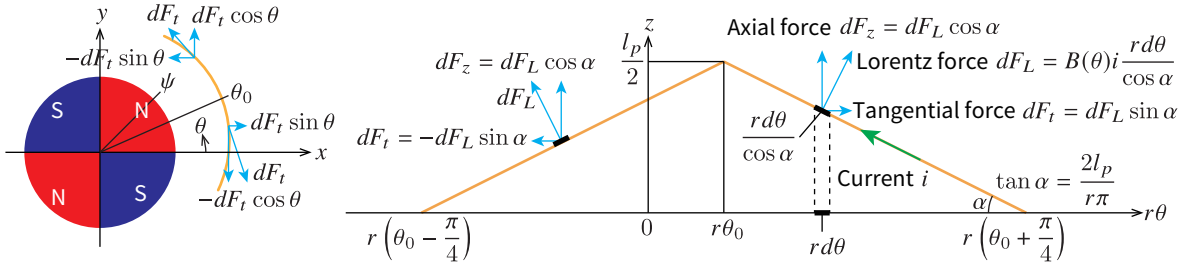

Figure 4: Coordinate of one-turn winding.

2.3 Analysis of force and torque

Next, the force and torque are analytically derived. Firstly, one-turn winding is considered and expanded into six-phase and N-turn winding.

The coordinate system is defined as Fig. 4. θ_0 is the angular position of the winding apex, and ψ is the rotational angle of the rotor. Assuming the magnetic flux density distribution to be

$$B(\theta) = B_r \cos 2(\theta - \psi) \tag{1}$$

where B_r is the amplitude of the magnetic flux density. Each phase current is expressed as

$$i_k = I_z \cos 2\left(\psi - \frac{\pi}{3}k\right) + I_m \sin 2\left(\psi - \frac{\pi}{3}k\right) + I_x \cos 2\left(\psi + \frac{\pi}{6}k\right) + I_y \sin 2\left(\psi + \frac{\pi}{6}k\right) \tag{2}$$

where $k = 0,1,2,3,4,5$ which corresponds to phase a, b, c, d, e, and f.

The Lorentz force at θ is calculated as Fig. 4, then the axial force by the one-turn winding is calculated as

$$F_{z0} = \int_{\theta_0 - \frac{\pi}{4}}^{\theta_0 + \frac{\pi}{4}} dF_z = rB_r \cos 2(\psi - \theta_0)\, i \tag{3}$$

Each phase winding is placed with the angular space of $\pi/3$, then the axial force of the one-turn six-phase winding becomes

$$F_{z1} = rB_r \sum_{k=0}^{5} \cos 2\left(\psi - \theta_0 - \frac{\pi}{3}k\right) i_k = 3rB_r \left(I_z \cos 2\theta_0 + I_m \sin 2\theta_0\right) \tag{4}$$

When the turn number is N, the angular space of each turn is $\pi/(3N)$. Then, the angular position of n-th winding is

$$\theta_n = -\frac{\pi(N-1)}{6N} + \frac{\pi}{3N}(n-1) \tag{5}$$

where the center of a-phase is set to 0. Since the force acted to the rotor is the reaction of the Lorentz force, the total axial force is calculated as

$$F_z = -3rB_r \sum_{n=1}^{N} \left(I_z \cos 2\theta_n + I_m \sin 2\theta_n\right) = -\frac{3\sqrt{3}rB_r}{2\sin\frac{\pi}{3N}} I_z \tag{6}$$

I_z generates a downward force in the lower winding while an upward force in the upper winding. Therefore, the opposite current should be supplied to control the axial force.

The tangential force of the one-turn winding is calculated as

$$f_{t0} = -\int_{\theta_0 - \frac{\pi}{4}}^{0} df_t + \int_{0}^{\theta_0 + \frac{\pi}{4}} df_t = \frac{2B_r l_p}{\pi} \sin 2(\psi - \theta_0)\, i \tag{7}$$

Calculating the rotational torque of the six-phase winding in the same way as the axial force, we have

$$T_{z1} = -r\frac{2B_r l_p}{\pi}\sum_{k=0}^{5}\sin 2\left(\psi-\theta_0-\frac{\pi}{3}k\right)i_k = \frac{6rB_r l_p}{\pi}\left(-I_z\sin 2\theta_0 + I_m\cos 2\theta_0\right) \tag{8}$$

and the rotational torque of N-turn winding is calculated as

$$T_z = \frac{6rB_r l_p}{\pi}\sum_{n=1}^{N}\left(-I_z\sin 2\theta_n + I_m\cos 2\theta_n\right) = \frac{3\sqrt{3}rB_r l_p}{\sin\frac{\pi}{3N}}I_m \tag{9}$$

The rotational torque can be controlled by I_m and is not affected by other currents.

The radial forces of the one-turn winding are calculated as

$$f_{x0} = \int_{\theta_0-\frac{\pi}{4}}^{0} df_t\sin\theta - \int_{0}^{\theta_0+\frac{\pi}{4}} df_t\sin\theta = -\frac{B_r l_p}{3\pi}\left\{(2+\sqrt{2})\cos(2\psi-3\theta_0) - 3(2-\sqrt{2})\cos(2\psi-\theta_0)\right\}i \tag{10}$$

$$f_{y0} = -\int_{\theta_0-\frac{\pi}{4}}^{0} df_t\cos\theta + \int_{0}^{\theta_0+\frac{\pi}{4}} df_t\cos\theta = \frac{B_r l_p}{3\pi}\left\{(2+\sqrt{2})\sin(2\psi-3\theta_0) + 3(2-\sqrt{2})\sin(2\psi-\theta_0)\right\}i \tag{11}$$

Then the forces of the six-phase winding are

$$\begin{aligned} f_{x1} &= -\frac{B_r l_p}{3\pi}\sum_{k=0}^{5}\left\{(2+\sqrt{2})\cos\left(2\psi-3\theta_0-\pi k\right) - 3(2-\sqrt{2})\cos\left(2\psi-\theta_0-\frac{\pi}{3}k\right)\right\}i_k \\ &= -\frac{3(2-\sqrt{2})B_r l_p}{\pi}\left(I_x\cos\theta_0 + I_y\sin\theta_0\right) \end{aligned} \tag{12}$$

$$\begin{aligned} f_{y1} &= \frac{B_r l_p}{3\pi}\sum_{k=0}^{5}\left\{(2+\sqrt{2})\sin\left(2\psi-3\theta_0-\pi k\right) + 3(2-\sqrt{2})\sin\left(2\psi-\theta_0-\frac{\pi}{3}k\right)\right\}i_k \\ &= \frac{3(2-\sqrt{2})B_r l_p}{\pi}\left(I_y\cos\theta_0 - I_x\sin\theta_0\right) \end{aligned} \tag{13}$$

and the forces with N-turn winding are

$$f_x = \frac{3(2-\sqrt{2})B_r l_p}{\pi}\sum_{n=1}^{N}\left(I_x\cos\theta_n + I_y\sin\theta_n\right) = \frac{3(2-\sqrt{2})B_r l_p}{\pi\sin\frac{\pi}{3N}}I_x \tag{14}$$

$$f_y = -\frac{3(2-\sqrt{2})B_r l_p}{\pi}\sum_{n=1}^{N}\left(I_y\cos\theta_n - I_x\sin\theta_n\right) = -\frac{3(2-\sqrt{2})B_r l_p}{\pi\sin\frac{\pi}{3N}}I_y \tag{15}$$

The radial forces can be controlled by I_x and I_y, respectively.

3. Experimental verification

To verify that the proposed method can control the bearing forces, a levitation test was conducted on a test machine.

The test machine is shown in Fig. 5. For simple fabrication, rectangular magnets are used. Windings are made by hand winding, and attached to the casing made from engineering plastic. Fig. 5 (c) is the appearance without the upper displacement sensors. The amplitude of the fundamental component of the magnetic flux density is approximately 0.32 T from the FEM results, then the axial force is calculated as 0.82 N/A for each winding from Eq. (6). The requirement for levitation, 1.62 N, can be generated.

Fig. 6 shows the control system. Five displacement sensors are installed. Linear amplifiers are used to supply the current. Fig. 7 shows the controllers. PD controllers with approximate differentiators are used. The

Figure 5: Test machine.

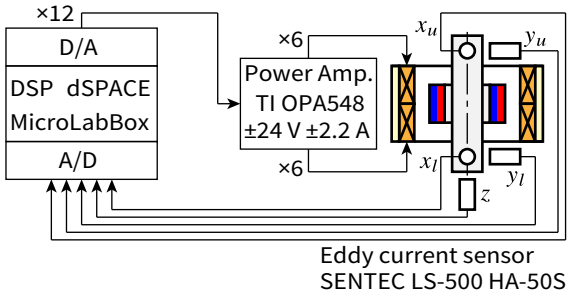

Figure 6: Control system.

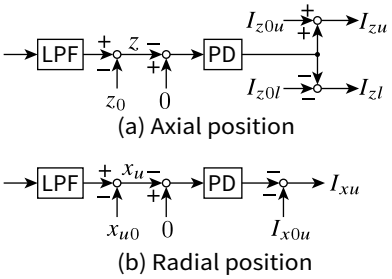

Figure 7: Controller.

Table 1: Parameters of controller

Proportional gain	2 A/mm	Break frequency of PD	500 Hz	Sampling time	0.1 ms
Differential gain	0.01 As/mm	Cutoff frequency of LPF	250 Hz		

controllers are converted to the discrete transfer functions by the Tustin method and implemented in the DSP. The upper and lower windings use different bias currents in the axial position control. Since the upper winding generates the attractive force while the lower winding generates the repulsive force, the rotational direction will be unstable if the same current is applied. Therefore, we reduce the bias current in the lower winding to stabilize the rotational position. The radial positions x_u, y_u, x_l, and y_l are controlled separately as shown in Fig. 7 (b). The gains, reference positions, and bias currents are tuned by trial and error in the experiment. The parameters of the controller are shown in Table 1. The same values are used for all PD controllers.

The startup responses are shown in Fig. 8. The displacement of the rotor is well controlled, and the rotor weight is supported by the stator currents. I_{z0u} and I_{z0l} were set to 1.4 A and 0.9 A, respectively. Since the average is 1.15 A, the axial force gain is 1.4 N/A, which is the almost same value as the theoretical value. These results confirm that the rotor can be actively supported in five axes by the proposed method.

4. Conclusions

A Lorentz-force-type self-bearing motor that controls both radial and axial forces is proposed, and its feasibility is demonstrated by theoretical analysis and experiments.

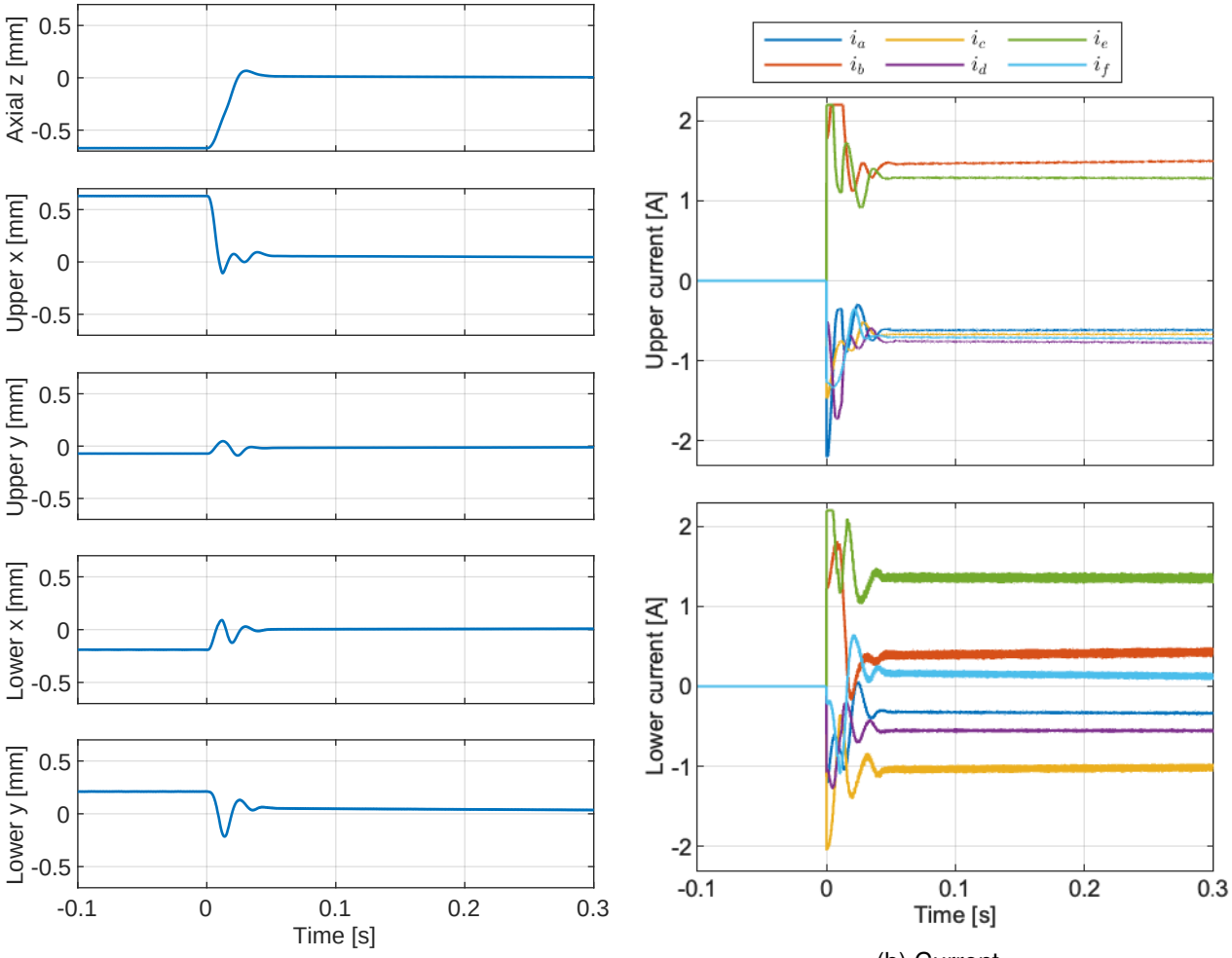

(a) Displacement

(b) Current

Figure 8: Startup responses of the rotor displacement and currents.

Acknowledgment

This work was partially supported by Tsugawa Foundation.

References

Osa, M., Masuzawa, T., Yamaguchi, K. & Tatsumi, E. (2021), 'Double stator axial gap type ultra-compact 5-dof controlled self-bearing motor for rotary pediatric ventricular assist device', *IEEE Transactions on Industry Applications* **57**(6), 6744–6753.

Ren, Z. & Stephens, L. (2005), 'Closed-loop performance of a six degree-of-freedom precision magnetic actuator', *IEEE/ASME Transactions on Mechatronics* **10**(6), 666–674.

Steinert, D., Nussbaumer, T. & Kolar, J. W. (2014), 'Slotless bearingless disk drive for high-speed and high-purity applications', *IEEE Transactions on Industrial Electronics* **61**(11), 5974–5986.

Ueno, S., Uematsu, S. & Kato, T. (2009), 'Development of a Lorentz-Force-Type Slotless Self-Bearing Motor', *Journal of System Design and Dynamics* **3**(4), 462–470.